JGR Atmospheres

RESEARCH ARTICLE
10.1029/2024JD042568

Chlorine Activation in Marine Air: Insights From Chemical Budgets of Molecular Chlorine and Hypochlorous Acid

Men Xia[1,2,3,4], Yifan Jiang[1], Jianing Dai[1], Yongchun Liu[3], Chao Yan[4,5], Markku Kulmala[2], and Tao Wang[1]

[1]Department of Civil and Environmental Engineering, The Hong Kong Polytechnic University, Hong Kong, China, [2]Faculty of Science, Institute for Atmospheric and Earth System Research/Physics, University of Helsinki, Helsinki, Finland, [3]Aerosol and Haze Laboratory, Beijing Advanced Innovation Center for Soft Matter Science and Engineering, Beijing University of Chemical Technology, Beijing, China, [4]Nanjing-Helsinki Institute in Atmospheric and Earth System Sciences, Nanjing University, Suzhou, China, [5]Joint International Research Laboratory of Atmospheric and Earth System Research (JirLATEST), School of Atmospheric Sciences, Nanjing University, Nanjing, China

Abstract Chlorine chemistry considerably affects air quality and climate in marine environments. Nitrogen oxides (NO_x), emitted by ocean-going vessels, react with sea salt chloride to generate reactive chlorine species. However, the exact mechanisms and chemical budget of chlorine remain poorly understood. In this study, we explore chlorine activation through field observations in Hong Kong, complemented by box modeling. Over the 2-week measurement period, the summer monsoon introduced abundant NO_x, producing molecular chlorine (Cl_2, 0.64 ± 0.69 ppt) and hypochlorous acid (HOCl, 8.9 ± 5.1 ppt). Daytime Cl_2 production was attributable to nitrate (NO_3^-) photolysis and the uptake on hydroxyl radicals (OH·) on chloride-containing aerosols. A budget analysis using the box model revealed that the production rate of HOCl, primarily driven by chlorine nitrate ($ClONO_2$) hydrolysis, was substantially lower than its loss rate. This discrepancy indicates either uncertainties in known HOCl sources or a missing source of chlorine atoms (Cl·). We examined the potential precursors of Cl· by incorporating emerging reactive chlorine species, such as, trichloramine (NCl_3) and iodine chloride (ICl), into the model. However, the inclusion of NCl_3 caused an overestimation of ambient Cl_2 levels, while adding ICl led to excessive ozone (O_3) depletion. Incorporating an unknown Cl· source (equivalent to ∼46 ppt Cl_2) remarkably enhanced atmospheric oxidation capacity, increasing daytime OH· levels by 12.8% and net ozone production by 35.7% while decreasing the mercury (Hg) lifetime by a factor of 3. These findings highlight the incomplete understanding of chlorine chemistry and suggest the existence of unidentified Cl· sources in coastal environments.

Plain Language Summary HOCl and Cl_2 are reactive chlorine species in the air, releasing highly reactive Cl· radicals in the presence of sunlight. Cl· reacts with various air pollutants, affecting air quality and climate. This study investigates the sources and impacts of HOCl and Cl_2 through field observations coupled with box modeling. First, we presented the time series, diurnal patterns, and correlation analysis of reactive chlorine. Next, we applied a box model to calculate the detailed chemical processes and evaluate the impact of chlorine chemistry. Results show that HOCl and Cl_2 were produced mainly through photochemical reactions, the rates of which were lower than their loss pathways including photolysis and depositions. The shortfall in the sources of HOCl and Cl_2 pointed to a missing source of Cl·. Furthermore, we discussed the candidates (NCl_3 and ICl) that could potentially contribute to the missing source. When considering the missing source of Cl· in the model, the impact of chlorine chemistry on secondary air pollution was significantly promoted. This study provides insights into the characteristics and roles of chlorine chemistry in coastal environments and calls for further studies of chlorine-containing species in the marine air.

Key Points:

- We performed field observations and box modeling of reactive chlorine species (Cl_2, HOCl, and $ClNO_2$) at a coastal site in Hong Kong, China
- Cl_2 was predominantly produced by nitrate photolysis and OH· uptake on aerosol, while HOCl was produced primarily via $ClONO_2$ hydrolysis
- A significant missing source of HOCl suggests the presence of unidentified Cl· radical sources at the observation site

Supporting Information:

Supporting Information may be found in the online version of this article.

Correspondence to:

T. Wang and M. Xia,
tao.wang@polyu.edu.hk;
men.xia@nju.edu.cn

Citation:

Xia, M., Jiang, Y., Dai, J., Liu, Y., Yan, C., Kulmala, M., & Wang, T. (2025). Chlorine activation in marine air: Insights from chemical budgets of molecular chlorine and hypochlorous acid. *Journal of Geophysical Research: Atmospheres*, *130*, e2024JD042568. https://doi.org/10.1029/2024JD042568

Received 27 SEP 2024
Accepted 20 FEB 2025

Author Contributions:

Conceptualization: Tao Wang
Data curation: Men Xia, Yifan Jiang
Formal analysis: Men Xia
Resources: Yongchun Liu, Markku Kulmala, Tao Wang
Validation: Chao Yan, Tao Wang
Visualization: Jianing Dai
Writing – original draft: Men Xia
Writing – review & editing: Men Xia, Tao Wang

1. Introduction

Chlorine atoms (Cl·), as potent oxidizers in the atmosphere, significantly influence the air quality and climate (Simpson et al., 2015). Cl· reacts with volatile organic compounds (VOCs) to produce peroxyl radicals (RO_2·, corresponding reaction presented as R1), which enhances ozone (O_3) production (R2–R3) and the formation of oxygenated organic molecules (OOMs) and secondary organic aerosols (SOA, R4) (Li et al., 2021; Y. Wang

et al., 2020). Moreover, Cl· consumes O_3 to produce chlorine monoxide (ClO·, R5). The net effect of chlorine chemistry typically enhances O_3 levels in polluted environments and depletes O_3 in remote areas such as the stratosphere and polar regions (Ma et al., 2023; Molina et al., 1987). Additionally, Cl· degrades methane (CH_4), altering the global lifetime of CH_4 and radiative forcing (Li et al., 2022). Lacking direct measurements of Cl·, current studies estimate the ambient concentration of Cl· by observing chlorine-containing species, for example, nitryl chloride ($ClNO_2$), molecular chlorine (Cl_2), and hypochlorous acid (HOCl), all of which releases Cl· upon photolysis (R6–R8).

$$Cl\cdot(g) + VOC(g) \rightarrow RO_2\cdot(g) + HCl(g) \quad (R1)$$

$$NO(g) + RO_2\cdot(g) = NO_2(g) + RO\cdot(g) \quad (R2)$$

$$NO_2(g) + O_2(g) + h\nu \rightarrow O_3(g) + NO(g) \quad (R3)$$

$$RO_2\cdot(g) + RO_2\cdot(g) \rightarrow OOMs \xrightarrow{\text{condense}} SOA \quad (R4)$$

$$Cl\cdot(g) + O_3(g) = ClO\cdot(g) + O_2(g) \quad (R5)$$

$$Cl_2(g) + h\nu = 2Cl\cdot(g) \quad (R6)$$

$$ClNO_2(g) + h\nu = Cl\cdot(g) + NO_2(g) \quad (R7)$$

$$HOCl(g) + h\nu = OH\cdot(g) + Cl\cdot(g) \quad (R8)$$

In the presence of nitrogen oxides (NO_x, NO + NO_2), chlorine chemistry is triggered by activating inert chlorine (i.e., particulate chloride, Cl^-) to reactive chlorine. NO_2 reacts with O_3 to successively produce the nitrate radical (NO_3·) and dinitrogen pentoxide (N_2O_5) (R9–R10). Laboratory studies have found substantial N_2O_5 uptake on chloride (Cl^-)-containing aerosols (R11–R13) that produce $ClNO_2$ (Finlayson-Pitts et al., 1989) and Cl_2 (Roberts et al., 2008). Furthermore, NO_2 facilitates chlorine cycling by reacting with ClO· to produce chlorine nitrate ($ClONO_2$) and hypochlorous acid (HOCl), which subsequently activate chloride on acidic aerosols to release Cl_2 (R14–R17). $ClONO_2$ can also undergo gas-phase homogeneous hydrolysis to produce HOCl (R18) (Atkinson et al., 1989).

$$NO_2(g) + O_3(g) = NO_3\cdot(g) + O_2(g) \quad (R9)$$

$$NO_3\cdot(g) + NO_2(g) = N_2O_5(g) \quad (R10)$$

$$N_2O_5(g) + Cl^-(aq) = ClNO_2(g) + NO_3^-(aq) \quad (R11)$$

$$N_2O_5(g) + 2Cl^-(aq) + 2H^+(aq) = Cl_2(g) + HONO(g) + HNO_3(aq) \quad (R12)$$

$$ClNO_2(g) + Cl^-(aq) + H^+(aq) = Cl_2(g) + HONO(g) \quad (R13)$$

$$ClO\cdot(g) + NO_2(g) = ClONO_2(g) + O_2(g) \quad (R14)$$

$$ClONO_2(g) + Cl^-(aq) + H^+(aq) = Cl_2(g) + HNO_3(aq) \quad (R15)$$

$$ClONO_2(g) + H_2O(aq) = HOCl(g) + HNO_3(aq) \quad (R16)$$

$$HOCl(g) + Cl^-(aq) + H^+(aq) = Cl_2(g) + H_2O(aq) \quad (R17)$$

$$ClONO_2(g) + H_2O(g) = HOCl(g) + HNO_3(g) \quad (R18)$$

Nitrogen oxide-assisted chlorine chemistry has been widely observed in various environments. The formation of $ClNO_2$ from N_2O_5 uptake was first discovered in the marine boundary layer and later in continental areas in the US, with mixing ratios ranging from several hundred ppt to a few ppb (Osthoff et al., 2008; Thornton et al., 2010). In continental outflows in Hong Kong, daytime Cl_2 levels can reach up to ~400 ppt on average, attributable to nitrate (NO_3^-) photolysis (Peng et al., 2022). NO_3^- photolysis produces the aqueous OH· radical, which can

oxidize chloride to produce Cl_2. Significant nocturnal correlations between $ClNO_2$ and Cl_2 have been observed in both East China and the US, indicating their common sources from N_2O_5 uptake (Haskins et al., 2019; Xia et al., 2020). These reactive chlorine species also participate in nitrogen oxide-influenced chlorine cycling in the coastal Arctic (McNamara et al., 2019) and during Australian wildfires (Solomon et al., 2023), demonstrating their widespread significance. However, fewer studies have focused on HOCl, except for one observation at Cape Verde (Lawler et al., 2011). Currently, known production pathways of HOCl include mainly $ClONO_2$ hydrolysis (R16) and the gas-phase reactions between ClO· and HO_2· (Molina et al., 1987). HOCl is mostly removed by photolysis, reactive uptake on aerosol, and deposition (Burkholder, 1993; Pratte & Rossi, 2006). As an intermediate species in chlorine cycling, ambient HOCl levels reflect the source strength of Cl·. However, the budget closure of the production and loss pathways of HOCl remains unclear, necessitating further investigation.

Ship emissions are a major source of NO_x in the marine boundary layer (Corbett & Fischbeck, 1997), potentially enhancing the chlorine chemistry initiated by sea salt production. In addition, ship engine exhaust contains VOCs and particulate matter (Corbett & Fischbeck, 1997), both of which contribute to chlorine chemistry by reacting with Cl· (R1) and providing reaction surfaces for $ClNO_2$ and HOCl uptake (R15–R17), respectively. Ship exhaust also emits nitrous acid (HONO), known to enhance atmospheric oxidation by releasing OH· upon photolysis (Gu et al., 2022). A recent modeling study incorporating HONO and $ClNO_2$ chemistry found that ship emissions can increase ozone (O_3) and $PM_{2.5}$ levels by 9%–21% and 7%–10%, respectively, in marine areas of East Asia (Dai & Wang, 2021). However, few field observations target reactive chlorine chemistry in ship-influenced marine air, limiting our understanding of the chlorine chemistry and atmospheric oxidation mechanisms in marine and coastal environments.

China is a global hotspot for ship emissions, with numerous international ports converging in the Pearl River Delta (PRD), facing the South China Sea (Zhang et al., 2017). Hong Kong, an important trade port in the PRD, hosts one of the busiest shipping lanes in the world (Yau et al., 2012). In this study, we present field observations from a coastal site in Hong Kong to examine the characteristics and chemistry of reactive chlorine, that is, $ClNO_2$, Cl_2, and HOCl, in ship emission-perturbed air masses under onshore wind flows. A chemical box model is used to analyze the chemical budget of reactive chorine and evaluate their impacts on atmospheric oxidation capacity. Furthermore, we assess the potential presence and impact of additional chlorine sources besides those observed. Overall, this study combines field observations with box modeling to investigate chlorine chemistry in the marine boundary layer with implications on air quality.

2. Methods

2.1. Observation Site and Period

Field observations were performed at the Cape D'Aguilar Supersite (CDSS), located at the southeast tip of Hong Kong Island in Hong Kong, China (Figure 1a). The CDSS is an air quality monitoring station that measures the regional background atmosphere in south China (S. Wang et al., 2019; T. Wang et al., 2019). The sampling site locates on a small hill, approximately 500 m from the nearest coastline, with ocean-going vessels (OGVs) visible from the site. The site is surrounded by evergreen broad-leafed trees and shrubs, contributing to biogenic emissions of VOCs. There are no obvious anthropogenic emission sources nearby, except for minimal traffic along a country road to the west. A small village named Hok Tsui, with a few dozen residents, is also located to the west of the sampling site. The observation period spanned from 16 to 28 August 2021, during which the dominant wind direction was south and southwest (Figure 1b). OGV emissions were the dominant anthropogenic sources of air pollutants during the field campaign.

2.2. Field Measurement Data

We conducted measurements of reactive chlorine species (i.e., $ClNO_2$, Cl_2, and HOCl) along with supporting data, including trace gases (O_3, carbon monoxide (CO), sulfur dioxide (SO_2), NO_x, HONO, and ammonia gas (NH_3)), the aerosol ionic composition (e.g., Cl^- and NO_3^- in $PM_{2.5}$) and size distributions, VOCs, meteorological parameters (wind speed, wind direction, temperature (T), and relative humidity (RH)), and the photolysis frequency of NO_2 (jNO_2) (Table S1 and Text S1 in Supporting Information S1).

We used an iodide-adduct high-resolution time-of-flight chemical ionization mass spectrometer (I^--HR-Tof-CIMS, Aerodyne Inc.) to simultaneously measure the gas-phase reactive chlorine species and reactive nitrogen

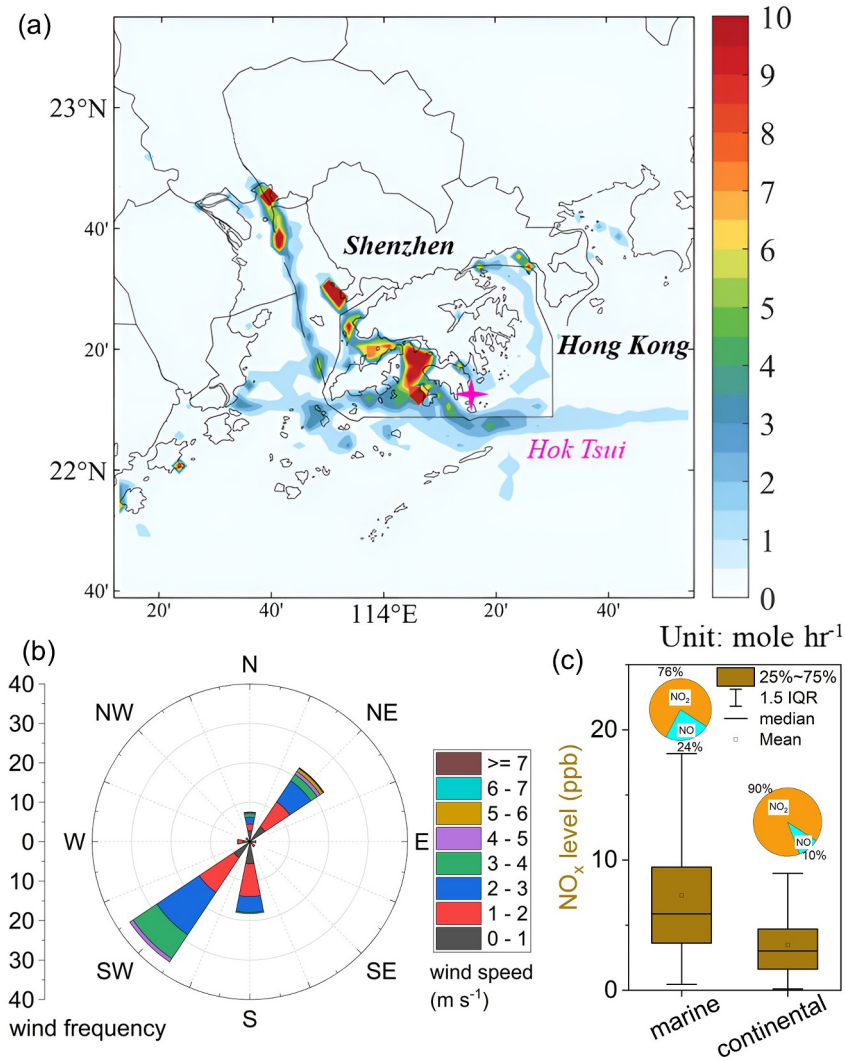

Figure 1. Overview of the sampling site with ship emissions and associated NO_x in Hong Kong, China. (a) NO_x emissions from ships (unit: mol hour^{-1}) in Hong Kong water in 2017 (data source: Hong Kong Environmental Protection Department, https://cd.epic.epd.gov.hk/, last visit: July 2024). The star marks our observation site in Hok Tsui. (b) Surface-level wind rose plot during the 2021 observation period. The left axis shows the frequency (unit: %) of wind from each wind sector. (c) NO_x levels in marine and continental air masses during the 2021 field campaign. The pie chart shows the proportion of NO and NO_2. IQR refers to the interquartile range.

(i.e., N_2O_5 and HONO). The principle of Tof-CIMS has been described in detail by Lee et al. (2014). An identical instrument was deployed at the same site in our previous work (Xia et al., 2022), and we adopted the same instrument configurations in the current study. Briefly, the Tof-CIMS uses iodide (I^-) and its water cluster (IH_2O^-) produced by the ionization of methyl iodide (CH_3I) as the reagent ions. I^- and IH_2O^- combine with target molecules (e.g., Cl_2 and HOCl) to produce iodide adducts (e.g., ICl_2^- and $IHOCl^-$), followed by detection in the mass spectrometer. More technical details regarding CIMS are shown as follows.

We used a perfluoro alkoxy (PFA) tubing (length: 0.5 m, outer diameter: 0.50 in., and inner diameter: 0.44 in.) as the sampling inlet. The sample residence time on the inlet was ~0.1 s. We did not use a water bubbler to humidify the ion-molecule reaction (IMR) chamber. We did not heat the IMR or inlet. This design was to minimize the hydrolysis or thermal decomposition of N_2O_5. The IMR pressure was maintained at 100 mbar. The potential inlet artifact was referred to our previous study using the same inlet configuration at the same site (Xia et al., 2022). In detail, 8% of N_2O_5 was lost on the sampling tube and converted to $ClNO_2$ (but no Cl_2). 13% of HOCl was lost on the inlet, while only 5% of the consumed HOCl was converted to Cl_2, contributing negligibly to ambient Cl_2

levels. Potential inlet conversion from $ClONO_2$ to HOCl was unlikely in this study, while future investigation of $ClONO_2$ is definitely needed (Text S2 in Supporting Information S1). These results suggest no significant inlet artifact using the current inlet settings. We checked the isotopic distribution of the detected clusters of reactive chlorine to verify the ambient measurements of these trace-level species. For example, the ambient signals of $I^{35}Cl^{35}Cl^-$ and $I^{37}Cl^{35}Cl^-$ were found strongly correlated and their ratios were relevant (determined by the natural isotopic ratio of ^{35}Cl and ^{37}Cl, Figure S1 in Supporting Information S1), which confirms the identity of Cl_2 and ensures accurate measurement in low ambient mixing ratios (e.g., 1–2 ppt).

We measured the background signals of the Tof-CIMS for 4 min every 3 hr, which were subtracted from their ambient signals (Text S1 and Figure S2 in Supporting Information S1). The background signal was measured by passing ambient air through a stainless steel tube (30-cm long and 0.5-inch inner diameter) filled with glass wool. The glass wool was soaked in NaOH solution (0.5 M) for 12 hr and dried before usage. Our laboratory test showed that targeted species, that is, N_2O_5, $ClNO_2$, Cl_2, HOCl, and HONO, contained in the airflow (2 Lpm, the same as the inlet flow of Tof-CIMS) can be absorbed by the tube with an efficiency higher than 99%. This stainless steel tube was connected to a solenoid valve together with the inlet tube of Tof-CIMS. We used a timer to control the solenoid valve so that ambient air can pass through the stainless steel tube for background measurement for 4 min in every 3 hr automatically. The Tof-CIMS sampled ambient air when not measuring the background. The detection limits were determined as three times of the standard deviation of the background signals, which were 0.28 ± 0.22 ppt for Cl_2, 0.35 ± 0.16 ppt for $ClNO_2$, and 0.55 ± 0.18 ppt for HOCl, and 0.99 ± 0.92 ppt for N_2O_5.

We performed laboratory calibrations for Cl_2, HOCl, and HONO, while on-site calibrations were performed for N_2O_5, $ClNO_2$, and Cl_2. Cl_2 was calibrated using a permeation tube (KIN-TEC) with a permeation rate of 110 ng min^{-1} at 40°C. HOCl-containing air used in the calibration was generated by injecting ultrapure nitrogen gas (N_2, 20 mL min^{-1}) through a phosphate-buffered sodium hypochlorite (NaOCl) solution (concentration: 2 mM and pH = 6.8). The HOCl-containing air was then passed through a cold Teflon tube (1/8-inch outer diameter, 0.065-inch inner diameter, 1 m length, and −20°C) with acidified NaCl droplets condensed onto its inner walls. The HOCl concentration was determined through complete conversion to Cl_2 and quantification of the generated Cl_2 levels by Tof-CIMS. N_2O_5 was synthesized by mixing NO_2 (in excess) with O_3, while $ClNO_2$ was generated by passing the synthesized N_2O_5 through a humidified NaCl slurry in a Teflon tube (1/2-inch outer diameter and 0.376-inch inner diameter). The ambient signal of HONO was calibrated by simultaneously injecting HONO-containing synthetic air into the Tof-CIMS and a long path absorption photometer (LOPAP, QUMA Elektronik & Analytic GmbH) (Heland et al., 2001). The HONO-containing air was produced by a HONO generator (QUMA, Model QS-03), and the injected HONO concentration was determined using the precalibrated LOPAP. The sensitivity of HONO, N_2O_5, $ClNO_2$, Cl_2, and HOCl under 70% RH were 0.27, 0.28, 1.35, 1.57 (consistent on-site and in laboratory), and 0.19 counts per second per ppt (cps ppt^{-1}), respectively, when the primary ion signals (both I^- and IH_2O^- considered) were normalized to 300,000 (average ambient level during our campaign). The ambient real-time primary ion signals were also normalized to 300,000 when deriving the mixing ratio. Other technical details of the Tof-CIMS and supporting measurements can be found in Text S1 of the Supporting Information S1.

2.3. Calculation of Kinetic Parameters

Kinetic parameters for reactive nitrogen and chlorine species were calculated to facilitate the analysis of the field observations, including the nocturnal steady-state lifetime of N_2O_5 ($\tau_{ss}(N_2O_5)$) (Brown et al., 2006), production efficiency of $ClNO_2$ ($\varepsilon(ClNO_2)$) (Eger et al., 2019), and photochemical parameters of NO_3^-.

The term $\tau_{ss}(N_2O_5)$ was calculated by dividing the N_2O_5 concentration by the production rate of NO_3 radicals ($P(NO_3)$), assuming that N_2O_5 achieves a steady state at night (Brown et al., 2006). A box modeling study shows relatively lower NO_2 concentrations and higher ambient temperature facilitates the achievement of N_2O_5's steady state (Brown et al., 2003), which is indeed the case in this study (average NO_2 mixing ratio: 5.0 ± 3.8 ppb and average T: 28.8 ± 2.4°C).

$$\tau_{ss}(N_2O_5) = \frac{[N_2O_5]}{P(NO_3)} = \frac{[N_2O_5]}{k_1[NO_2][O_3]} \quad (1)$$

where $[N_2O_5]$ represents the ambient N_2O_5 concentration, and k_1 denotes the temperature-dependent rate constant of the $NO_2 + O_3$ reaction.

The term $\varepsilon(ClNO_2)$ represents the proportion of the produced $NO_3\cdot$ radicals that is ultimately converted to $ClNO_2$. The definition of $\varepsilon(ClNO_2)$ used in this study is equivalent to the original definition by Eger et al. (2019), but the calculation (Equation 2) is performed in a simplified manner herein. As the $ClNO_2$ mixing ratio could show a fluctuating trend after the initial increase during the night, this definition of $\varepsilon(ClNO_2)$ actually represents a lower limit.

$$\varepsilon(ClNO_2) = \frac{(ClNO_2)_{max}}{\int_0^t P(NO_3)\,dt} = \frac{(ClNO_2)_{max}}{\int_0^t k_1[NO_2][O_3]\,dt} \quad (2)$$

where $(ClNO_2)_{max}$ denotes the maximum 5-min-averaged $ClNO_2$ concentration during the night, and t is the integration time (11 hr from sunset to sunrise) for the production of $NO_3\cdot$ radical. $[NO_2]$ and $[O_3]$ denote the ambient-observed concentrations of NO_2 and O_3, respectively.

We also calculated a NO_3^- photolysis indicator ($I(NO_3^-)$) and the NO_3^- photolysis rate ($R(NO_3^-)$). $I(NO_3^-)$ is an empirical parameter based on the multiplication of potential factors influencing NO_3^- photolysis, as derived in a previous study (Equation 3) (Peng et al., 2022), while $R(NO_3^-)$ represents the first-order loss rate of aerosol NO_3^- due to photolysis (Equation 4). $R(NO_3^-)$ and $I(NO_3^-)$ were used for correlation analysis with reactive chlorine but not for quantifying the Cl_2 production rate in the box model (Section 2.4).

$$I(NO_3^-) = jNO_2 \times Sa \times [NO_3^-] \quad (3)$$

where Sa is the aerosol surface area density ($\mu m^2\ cm^{-3}$) calculated using particle size distribution from 10 to 800 nm (Text S1 and Table S1 in Supporting Information S1). It should be noted that the coarse mode of the marine aerosol could not be taken into account in this calculation.

$$R(NO_3^-) = jNO_3^- \times [NO_3^-] \quad (4)$$

where jNO_3^- is the photolysis frequency (s^{-1}) of aqueous-phase NO_3^-, computed using the tropospheric ultraviolet-visible (TUV) radiation model, assuming a unity quantum yield (https://www.acom.ucar.edu/Models/TUV/Interactive_TUV/; last access: May 2024). The aerosol pH, defined as the negative logarithm of the aqueous H^+ concentration ($-\log_{10}([H^+])$, $[H^+]$ unit: mol L^{-1}), was calculated using a thermodynamic model, ISORROPIA II (Fountoukis & Nenes, 2007). Additional technical details of these parameters can be found in Text S3 of the Supporting Information S1.

2.4. Chemical Box Model

We applied the framework for zero-dimensional (0-D) atmospheric modeling (F0AM) to analyze the budget of reactive chlorine and evaluate the impact of ship emissions on atmospheric oxidation capacity (Wolfe et al., 2016). As an observation-based chemical box model, F0AM incorporates the master chemical mechanism (MCM v3.3.1) as the default chemical mechanism (Jenkin et al., 2015). MCM involves near-explicit reactions of VOCs, trace gases (e.g., CO, NO_x, and O_3), and radicals (e.g., $OH\cdot$, $HO_2\cdot$, and $RO_2\cdot$) in the gas phase. We incorporated an additional chemical module to account for the gas-phase chemistry of reactive chlorine. This additional module, developed in our previous study, includes gas-phase reactions involving $Cl\cdot$ radicals, O_3, and VOCs, as well as a simplified heterogeneous module (Xia et al., 2022).

Further to those established mechanisms, we compiled the gas-phase degradation mechanisms of trichloramine (NCl_3) and iodine chloride (ICl) and implemented these modules to explore potential $Cl\cdot$ sources, respectively (Tables S2 and S3 in Supporting Information S1). The NCl_3 module consists of multiple-step NCl_3 photolytic degradation, producing Cl_2 and $Cl\cdot$. In detail, NCl_3 photolysis produces $NCl_2\cdot$ radicals, which can either react with itself or react with NCl_3. The ICl module contains ICl photolysis and subsequent iodine chemistry, especially complex interactions associated with O_3 (Saiz-Lopez et al., 2014). A total of 51 reactions are included to account for the effect of ICl photolysis. On one hand, some reactions consume O_3, for example, the $I\cdot + O_3$ reaction. On

the other hand, some reactions facilitate O_3 production, for example, the IO· radical converts NO to NO_2. These modules were applied separately in the model, with NCl_3 or ICl concentrations constrained to specific levels (Section 3.3, Table S5 in Supporting Information S1). In the individual model run, a constant mixing ratio was used for NCl_3 or ICl for lack of knowledge in their diurnal profiles.

The model was constrained using 10-min resolution data (Table S4 in Supporting Information S1) for the entire observation period. Observations from the first day were repeated three times to stabilize the intermediates (mostly unconstrained radicals) in the model, while only the results from the last run for the first day, along with subsequent days, were adopted for further analysis. The simulated radical concentrations (OH·, Cl·, and NO_3·) were extracted to calculate the VOC oxidation rates associated with each oxidant and the lifetime of gaseous elemental mercury (Hg^0) (Xia et al., 2022). The net O_x (=O_3 + NO_2) production rate ($P(O_x)$) was calculated as described in our prior study (Xia et al., 2022). We configured four cases to differentiate the contributions of reactive chlorine and HONO to OH· and O_3 production (Table S5 in Supporting Information S1):

1. The "base" case, excluding both reactive chlorine and HONO;
2. The "with Cl" case, including reactive chlorine but excluding HONO;
3. The "with Cl and HONO" case, including both reactive chlorine and HONO; and
4. The "with additional Cl" case, incorporating potential chlorine sources from additional Cl_2 photolysis (Section 3.3).

Additionally, we performed sensitivity tests to examine the response of OH· levels and the net O_x production to changes in other species or environmental conditions. The sensitivity was quantified based on the relative incremental reactivity (RIR) (Zheng et al., 2023). RIR_OH was calculated as the percentile change in the OH· concentration divided by the percentile changes in the environmental factors. A similar approach was applied to determine RIR_net $P(O_x)$. Details of RIR calculations are presented in Supporting Information S1 (Text S4).

3. Results and Discussion

3.1. Overall Observations

The field campaign in Hong Kong observed perturbed marine air masses with ship emissions along with minor influence from continental urban areas (Figure 1b). The intercepted air was warm (T) and humid (RH), with low levels of particulate matter ($PM_{2.5}$ 4.2 ± 2.2 μg m^{-3}, campaign average, Figure 2). However, we observed elevated levels of NO_x throughout the campaign (Figure 1c). The diurnal pattern of NO showed a morning peak at 10:00 (local time), while NO_2 exhibited a nighttime peak with minimum concentrations from 10:00 to 15:00 (Figure S3 in Supporting Information S1). NO_x levels were obviously higher in marine-influenced air masses (6.4 ± 5.1 ppb, average ± standard deviation, mainly south and southwest) than those observed in occasional continental outflows (3.5 ± 2.7 ppb, mainly north and northeast, Figure 1c). The higher levels of NO_x in marine-influenced air are caused by more intense ship emissions west and southwest of the observation site (Figure 1a) and the sea-land breeze that brings NO_x to our field site (Figure S4 in Supporting Information S1). A comparison of the NO_x/SO_2 ratio with the previous study differentiates the pattern between marine air in this study and continental air (Figure S4 in Supporting Information S1).

We observed reactive chlorine species with discrepant diurnal patterns throughout the campaign (Figure 3). $ClNO_2$ displayed a typical nighttime peak, with an average mixing ratio of 18 ± 35 ppt. These $ClNO_2$ levels are substantially lower than those observed in continental outflows from the PRD (T. Wang et al., 2016) and Los Angeles (Riedel et al., 2012). The low concentrations of $ClNO_2$ are attributable to low levels of O_3, which limits the formation of N_2O_5 through the reaction of NO_2 and O_3. Moreover, the low levels of $PM_{2.5}$ indicate limited aerosol surface area available for N_2O_5 uptake and $ClNO_2$ production. Despite the low campaign-average level, the $ClNO_2$ mixing ratios exceeded 200 ppt on certain nights and exhibited considerable day-by-day variability. In contrast, both HOCl (8.9 ± 5.1 ppt, campaign average) and Cl_2 (0.64 ± 0.68 ppt) showed obvious daytime peaks with smooth variations, indicating photochemical production of these species. While the levels of reactive chlorine species (i.e., $ClNO_2$, Cl_2, and HOCl) observed in ship emission-perturbed marine inflows are considerably lower than those found in continental outflows at this site in previous studies (Peng et al., 2022; Xia et al., 2022), their diurnal patterns are consistent across both marine inflows and continental outflows. These results suggest that ship activities in the marine boundary layer trigger pollution-derived chlorine activation. The

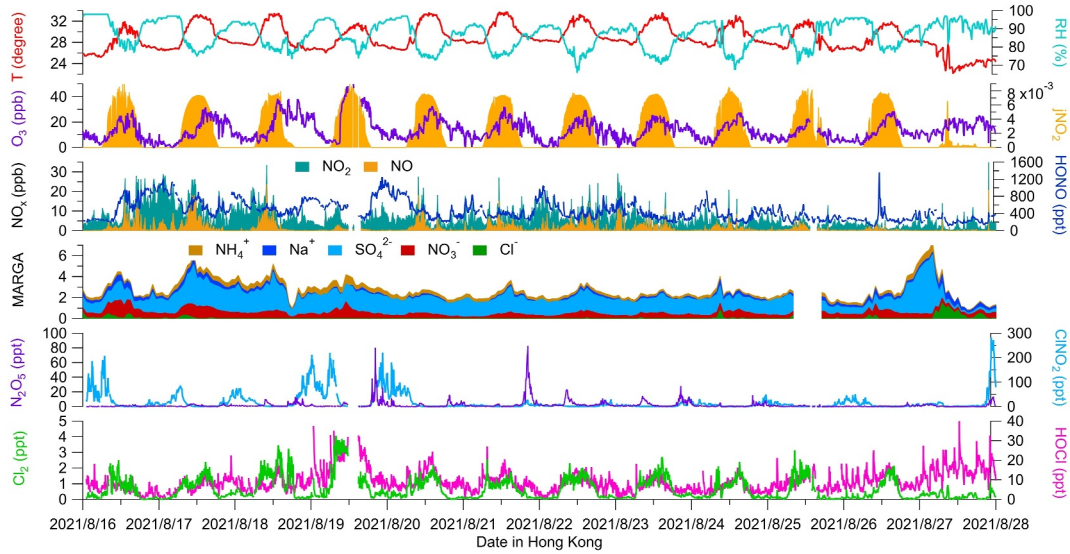

Figure 2. Overall time series of field observations in Hong Kong, China. The unit of $j\mathrm{NO_2}$ is $\mathrm{s^{-1}}$, while the unit of mass concentration of the ionic species measured by MARGA is μg $\mathrm{m^{-3}}$. The date and time show local time throughout this work. Additional observation data, for example, VOCs, are shown in Figure S5 of the Supporting Information S1 as average diurnal profiles.

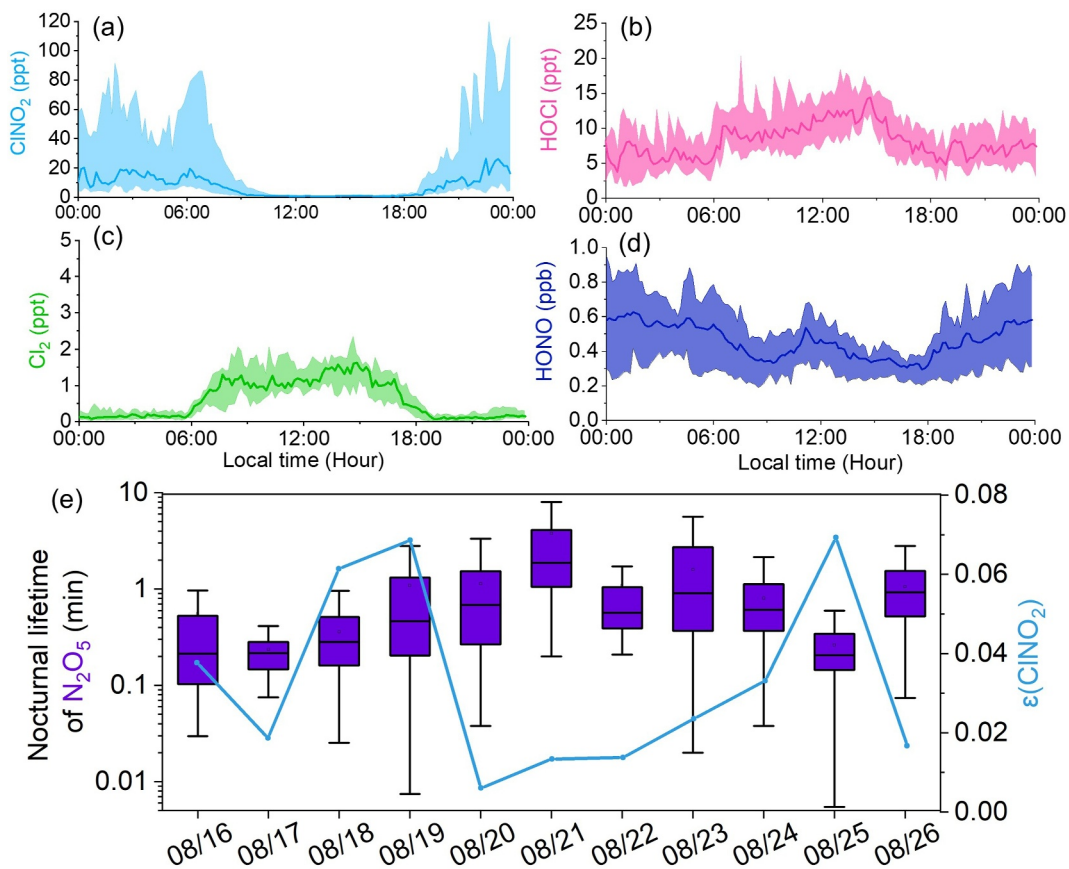

Figure 3. Diurnal patterns of radical precursors and kinetic parameters. The diurnal patterns were averaged from the entire field campaign. (a)–(c) Diurnal patterns of precursors of Cl· radicals, that is, $\mathrm{ClNO_2}$, HOCl, and $\mathrm{Cl_2}$, respectively. (d) Diurnal patterns of a major precursor of OH· radicals, HONO. (e) Nocturnal lifetime of $\mathrm{N_2O_5}$ ($\tau_{ss}(\mathrm{N_2O_5})$) and $\mathrm{ClNO_2}$ production efficiency ($\varepsilon(\mathrm{ClNO_2})$).

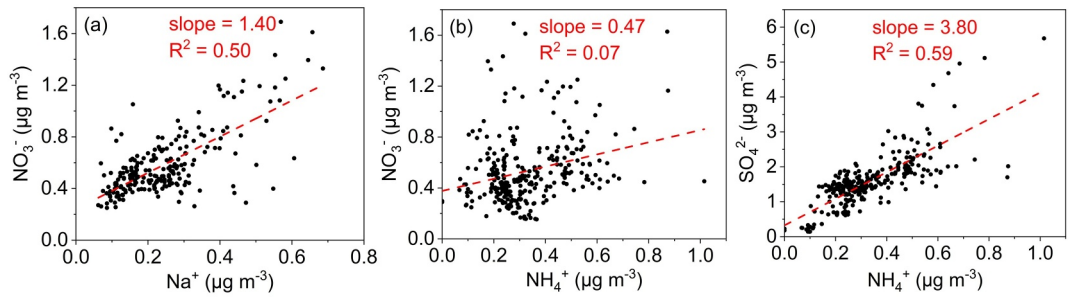

Figure 4. Correlation analysis of ionic compositions in $PM_{2.5}$. (a) Correlation between NO_3^- and Na^+. (b) Correlation between NO_3^- and NH_4^+. (c) Correlation between SO_4^{2-} and NH_4^+.

presence of HOCl and Cl_2 in the daytime implies an atmospheric source of Cl· radicals because both can be readily photolyzed, as discussed in subsequent sections.

We also detected abundant levels of reactive nitrogen species, which are relevant to the reactive chlorine species, including HONO, N_2O_5, and particulate NO_3^-. In particular, remarkable concentrations of HONO were observed, with an average mixing ratio of 0.46 ± 0.22 ppb. HONO photolysis releases OH·, which competes with Cl· in oxidizing VOCs. On the contrary, N_2O_5, another reservoir species of NO_x, showed much lower concentrations, ranging from 0 to 15 ppt in its diurnal pattern. Low levels of N_2O_5 at night limit $ClNO_2$ production, as previously discussed. Inorganic NO_3^- in $PM_{2.5}$ showed an obvious daytime peak, with average diurnal concentrations ranging from 0.3 to 1.5 μg m^{-3} (Figure S6 in Supporting Information S1). As NO_3^- and $ClNO_2$ are simultaneously produced following N_2O_5 uptake on aerosols during the night, the diurnal pattern of NO_3^- indicates limited nighttime chemistry. Conversely, elevated daytime NO_3^- levels, coupled with its photolysis, implies active photochemistry and potential chlorine activation during the daytime. The following section discusses the kinetics of ship emission-induced chlorine activations through nitrogen oxide-related chemistry.

3.2. Kinetic Parameters and Correlations

Following the overall observations and diurnal patterns, we calculated the kinetic parameters (Section 2.4) of reactive chlorine to further understand its characteristics. N_2O_5 is also discussed, as its heterogeneous loss is responsible for the nocturnal production of $ClNO_2$ and Cl_2 (Roberts et al., 2008). $\tau_{ss}(N_2O_5)$ mostly lies in the range of 0.1–10 min, indicating a rapid heterogeneous loss of N_2O_5 on aerosols (Z. Wang et al., 2017) or the ocean surface (Kim et al., 2014). This short lifetime of N_2O_5 is consistent with its low nocturnal concentrations. ε ($ClNO_2$) ranges from 0.01 to 0.07, similar to the values from previous shipborne measurements (Eger et al., 2019). This result shows that merely 1%–7% of the produced NO_3· radicals are converted to $ClNO_2$. Correspondingly, the rest of NO_3· is directly lost via reactions with NO and VOCs and is indirectly converted to particulate nitrate through producing N_2O_5 first. The low $\varepsilon(ClNO_2)$ can be attributed to high temperatures during our observations, which shift the NO_3·–N_2O_5 equilibrium toward NO_3·. Moreover, low $PM_{2.5}$ concentrations may limit the heterogeneous production of $ClNO_2$ on aerosol surfaces.

We also conducted correlation analysis of aerosol ionic compositions, focusing on relevant species of reactive chlorine (NO_3^- and Cl^-). The results show that particulate NO_3^- is significantly correlated with sodium (Na^+) ($R^2 = 0.5$, Figure 4a) and Cl^- ($R^2 = 0.57$) but barely correlated with ammonium (NH_4^+) ($R^2 = 0.07$, Figure 4b). In contrast, sulfate (SO_4^{2-}) is strongly correlated with NH_4^+ ($R^2 = 0.59$, Figure 4c). These results infer that NO_3^- could be mainly produced by the acid displacement of HNO_3 on sea salt aerosol (R19) instead of the reaction between HNO_3 and NH_3 (R20). The average aerosol pH estimated by the thermodynamic model is 2.1 ± 0.3 (Text S3 in Supporting Information S1), which is conducive for the combination of H^+(aq) and Cl^-(aq) to produce HCl (aq). Moreover, HCl(aq) tends to evaporate into the gas phase owing to the high temperature in summer. Smaller amounts of Cl^- in the aerosol phase could be a potential reason for the low levels of observed reactive chlorine.

$$NaCl(s) + HNO_3(g) = NaNO_3(s) + HCl(g) \quad (R19)$$

$$NH_3(g) + HNO_3(g) = NH_4NO_3(s) \quad (R20)$$

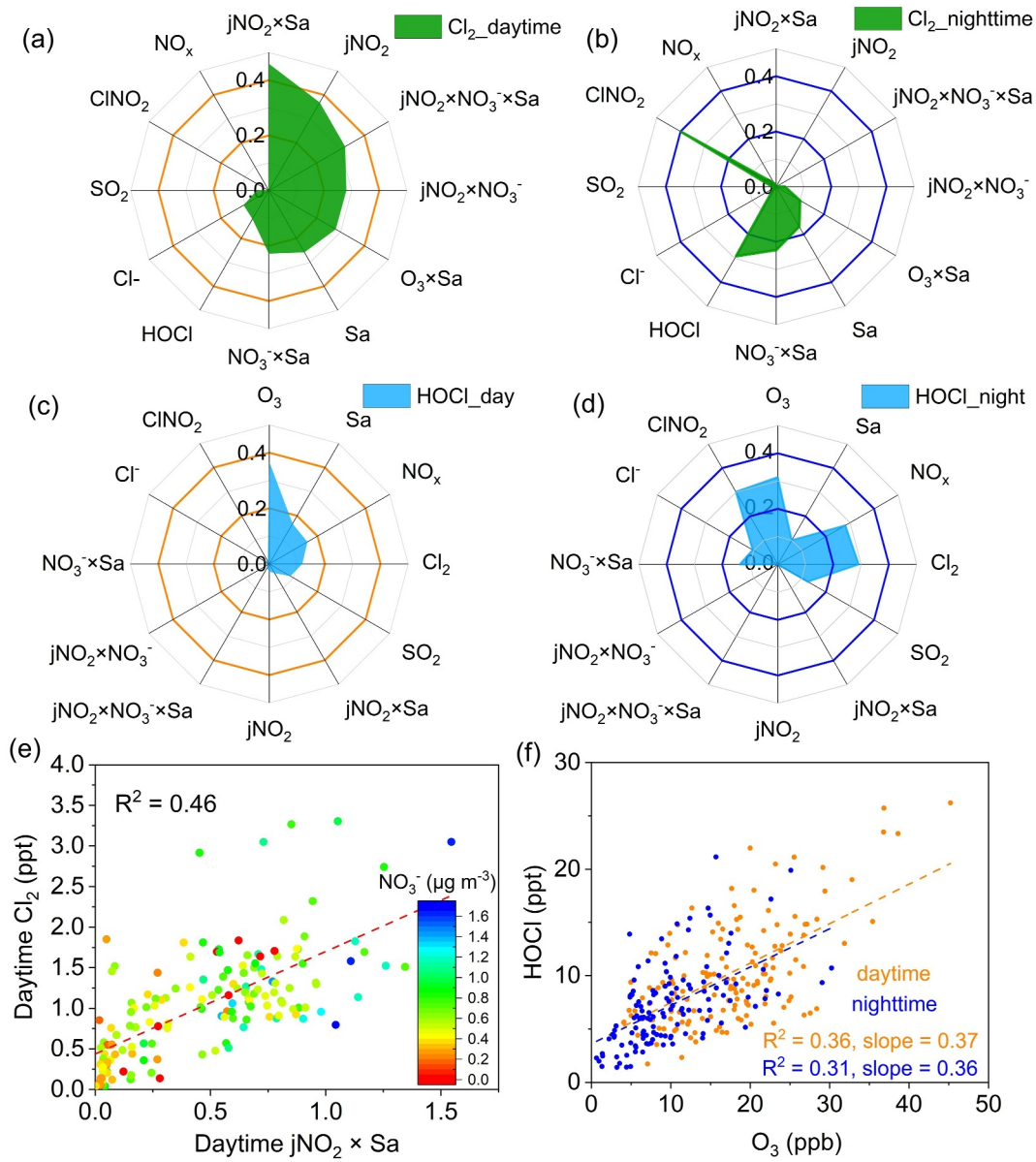

Figure 5. Correlation analysis of Cl_2 and HOCl. (a) and (b) display the correlation coefficients of Cl_2 with environmental factors during the daytime and nighttime, respectively. (c) and (d) show the same plots for HOCl. (e) and (f) show the scatter plot of Cl_2 or HOCl with the most relevant (i.e., with the largest R^2) species or parameters. In (f), the orange and blue dots indicate daytime and nighttime observations, respectively.

Cl_2 exhibits different correlations with other species or parameters. During the day, Cl_2 shows significant correlation with the parameter $jNO_2 \times Sa$ ($R^2 = 0.46$, Figures 5a and 5e), $jNO_2 \times Sa \times NO_3^-$, and $jNO_2 \times NO_3^-$, indicating Cl_2 production from photochemical sources (Peng et al., 2022). A weaker correlation between Cl_2 and $O_3 \times Sa$ ($R^2 = 0.28$) was also observed. Other pathways beyond our consideration, such as iron-catalyzed photochemical reactions on aerosols, may also contribute to Cl_2 production (Chen et al., 2024; Lim et al., 2006). At night, Cl_2 is significantly correlated with $ClNO_2$ ($R^2 = 0.40$, Figure 5b), consistent with previous laboratory studies and field observations (Roberts et al., 2008; Xia et al., 2020).

HOCl demonstrates the strongest correlations with O_3 during both day and night ($R^2 = 0.36$ and 0.31, respectively, Figures 5c, 5d, and 5f). The daytime HOCl–O_3 relationship is likely attributable to the HOCl production from the reaction between Cl· and O_3. Other sources, such as direct emissions and nitrate photolysis, are not related to daytime HOCl production. Additionally, daytime HOCl is independent of Cl_2. At night, HOCl is

correlated with NO_x, O_3, $ClNO_2$, and Cl_2 (R^2 0.28–0.31), indicating nighttime chemistry initiated by NO_3· radicals. In detail, NO_3· originated from NO_x initiates N_2O_5 production, which undergoes heterogeneous uptake to produce $ClNO_2$ and Cl_2. Furthermore, Cl_2 hydrolysis is one possible pathway for HOCl production. It should be noted that the above correlation analysis may contain uncertainties and are qualitative only.

3.3. Budget Analysis

The kinetic calculations and correlation analysis provide a qualitative understanding of the factors influencing reactive chlorine species. In this section, we present a more thorough analysis of their production and loss pathways through a budget analysis aiming at quantifying their fates. We selected Cl_2 and HOCl to perform this daytime budget analysis, as the daytime sources of Cl_2 and HOCl exhibit the highest uncertainties. The budget analysis for $ClNO_2$ was not conducted as the fate of $ClNO_2$ is more explicit, that is, production through N_2O_5 uptake alone and loss mainly via photolysis and depositions. The budget analysis was performed using a chemical box model based on diurnal averages of observation data (Section 2.3). Additional details of the box model are provided in Supporting Information S1 (Text S4).

The daytime sources of Cl_2 in the model include heterogeneous uptake on OH·, O_3, $ClONO_2$, and HOCl on chloride-containing aerosol and homogeneous reactions of Cl· + $ClONO_2$, ClO· + ClO·, and $ClONO_2$ + H_2O (Atkinson et al., 1989; L. Wang et al., 2015). It should be noted that ambient $ClONO_2$ was always below the instrument detection limit in this study. These chemical pathways are recognized as key secondary sources of Cl_2 with explicit kinetic parameters. Direct emissions of Cl_2 and HOCl were not included for lack of nearby emission sources, such as water treatment facilities or swimming pools. According to our simulations, the reactive uptake on OH· on aerosol surfaces is the most critical source of Cl_2 production (Figure 6a) among these pathways. The significance of the OH· uptake rate could be attributable to the elevated OH· levels simulated by the model (1.5×10^7 molecule cm^{-3} at noon) and the large OH· uptake coefficient (0.2) reported previously (Ammann et al., 2013). The second most significant source of Cl_2 is the reactive uptake on HOCl (uptake coefficient: 2×10^{-4}) on acidic, chloride-containing particles (Ammann et al., 2013). This pathway suggests chlorine cycling instead of a net production of Cl_2 considering the interconversion of HOCl and Cl_2 (R12 and R15–R16). O_3 uptake (uptake coefficient: 7.7×10^{-8}) plays a minor role in Cl_2 production, consistent with our correlation analysis (Ammann et al., 2013). Other known pathways contribute little to Cl_2 formation. Contrary to its complicated formation pathway, Cl_2 loss is dominated by photolysis alone (>99% contribution).

Theoretically, ambient Cl_2 should reach a photochemical steady state due to its rapid photolysis and short photochemical lifetime (~6 min at zero solar zenith angle in clear-sky conditions). A steady state of Cl_2 means equal production and loss rates of Cl_2. However, we found an obvious shortfall in Cl_2 sources, equivalent to ~50% of total Cl_2 losses. The gap in Cl_2 sources could be caused by uncertainties in the uptake coefficients of OH· and HOCl or in the model-simulated OH· concentrations. Alternatively, other known Cl_2 sources that are not constrained in the model could fill in the shortfall, including chloride oxidation induced by nitrate photolysis and iron-catalyzed reactions (Abbatt et al., 2010; Chen et al., 2024). These processes were excluded from the model for lack of explicit kinetic parameters. Specifically, the rate constant of nitrate photolysis varies by several orders of magnitude, according to laboratory studies using aerosol filters (Ye et al., 2016), while the rate constant of iron-catalyzed Cl_2 depends on aerosol Fe(III) concentrations ($[Fe^{3+}]$), which were not measured in this study.

We further examined the correlation between the missing source of Cl_2 and other species or parameters. Results showed that the missing source of Cl_2 had no correlation with NO_x or SO_2 (Figures 6b and 6c), ruling out primary emissions from shipping activities or regional coal burnings as potential contributors. The missing source of Cl_2 exhibits weak correlations with O_3 and HOCl (Figures 6d and 6e) while shows significant relationship with the indicator of NO_3^- photolysis ($I(NO_3^-)$ and $R^2 = 0.54$, Figure 6f). Interestingly, this correlation improves slightly ($R^2 = 0.70$ and slope = 0.021, Figure 6g) when the NO_3^- photolysis rate ($R(NO_3^-)$) is used instead of $I(NO_3^-)$. Furthermore, the slope (0.021) in Figure 6g represents the production yield of Cl_2 from NO_3^- photolysis, assuming that the majority of the Cl_2 missing source is attributable to NO_3^- photolysis. Aerosol iron photochemistry has recently been proposed as a potential source of Cl_2 in North China (Chen et al., 2024). However, the broader significance of iron photochemistry for Cl_2 production remains unclear, and the iron concentrations in aerosol have not been measured in this study. Nevertheless, iron photochemistry could be important in ship emission plumes, as previous studies have reported iron-bearing aerosol emissions from ship exhaust (Fu

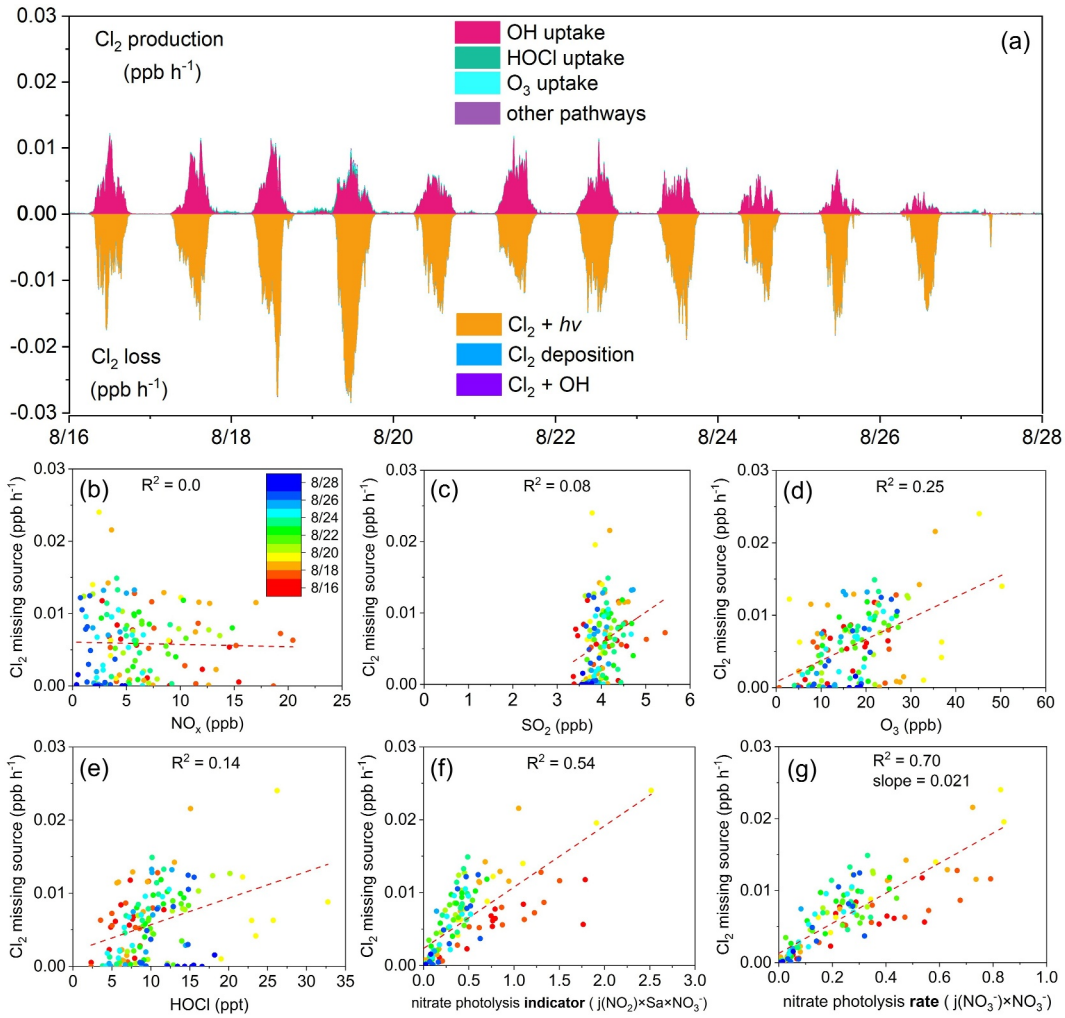

Figure 6. Cl_2 budget and missing source. (a) Cl_2 budget (i.e., production and loss pathways) during the field campaign. (b)–(g) Correlation of the missing source of Cl_2 with environmental factors: (b) NO_x, (c) SO_2, (d) O_3, (e) HOCl, (f) the nitrate photolysis indicator, $I(NO_3^-)$, and (g) the nitrate photolysis rate, $R(NO_3^-)$, unit: ppb h^{-1}.

et al., 2014). Overall, the contribution of iron photochemistry to Cl_2 production in Hong Kong, although not quantitatively discussed here, warrants further research.

We also analyzed the budget of HOCl. Among the known sources, HOCl is predominantly produced by the homogeneous hydrolysis of $ClONO_2$, favored by the abundance of water vapor. The chemical budget of ClO· (Figure S7 in Supporting Information S1) exhibits that its net consumption proceeds predominantly via the reaction with NO_2 to produce $ClONO_2$, while the ClO· and HO_2· reaction to produce HOCl is less significant. Other known sources of HOCl, such as the heterogeneous hydrolysis of $ClONO_2$ on aerosols, are negligible due to the limited aerosol surface area. Notably, additional HOCl production from NO_3^- photolysis is unlikely, as laboratory studies have revealed that NO_3^- photolysis mainly produces Cl_2 rather than HOCl (Peng et al., 2022). Direct emissions of HOCl could also be excluded, consistent with our discussion on Cl_2 sources. In terms of HOCl loss, photolysis alone accounts for over 90%, outweighing other pathways such as HOCl uptake on aerosol and deposition. In summary, the budget analysis of HOCl reveals an even larger missing source of HOCl (>90%) than Cl_2. As the secondary production of HOCl originates from Cl·, the missing source of HOCl probably indicates missing sources of Cl·.

Recently, additional reactive chlorine species have been observed in ambient air, that is, chloramines (e.g., NCl_3) and ICl, which can act as Cl· precursors (Tham et al., 2021; C. Wang et al., 2023). NCl_3 can be emitted from water treatment and produced secondarily, while ICl is mainly produced by hypoiodous acid (HOI) uptake on chloride

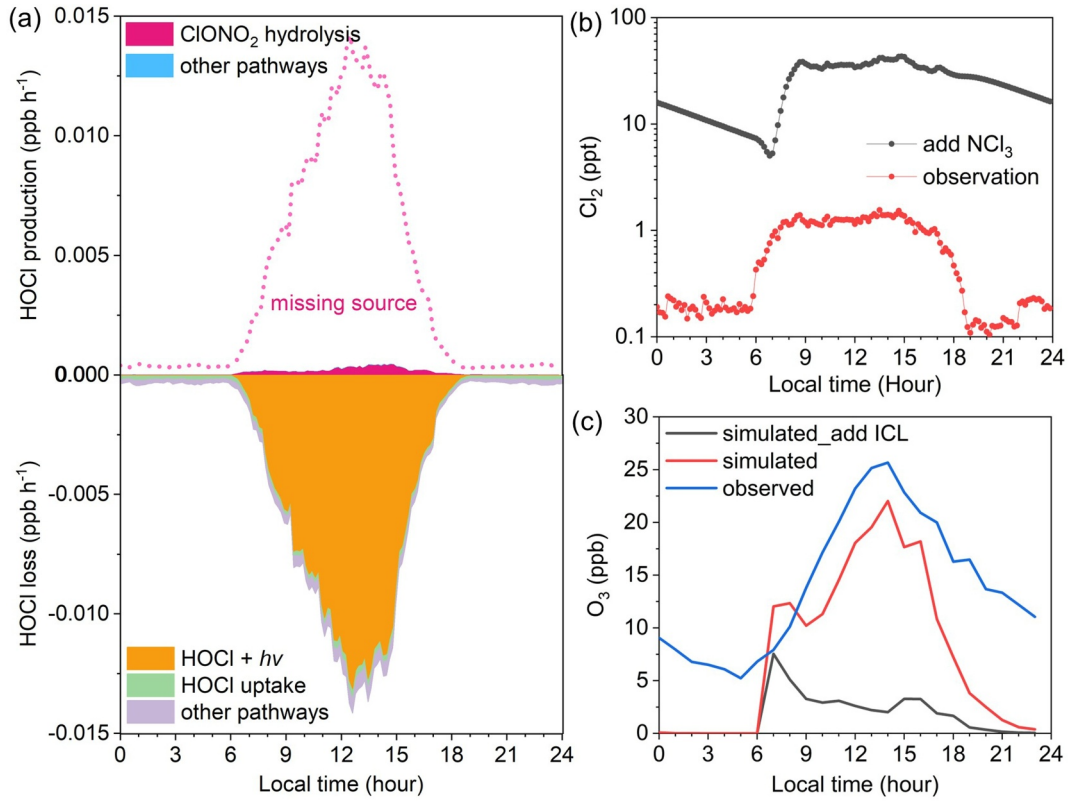

Figure 7. Budget analysis of HOCl and investigation of potential chlorine precursors during campaign-average conditions. (a) Production and loss pathways of HOCl simulated without additional chlorine sources. (b) Cl_2 levels simulated by incorporating NCl_3 into the box model and comparison with field observations. (c) Comparison of O_3 levels under three scenarios: (1) ambient observation, (2) simulation using the observed data, and (3) simulation by incorporating ICl with observations.

aerosols. We explored the possibilities of this emerging reactive chlorine as a potential Cl· source by incorporating them into the box model to assess their effects (see Section 2.4). We iteratively adjusted the constrained level of NCl_3 or ICl in the model until the HOCl production balanced its loss (Figure S8 in Supporting Information S1). The results show that 16.3 ppt of NCl_3 would be required to account for the missing HOCl source. However, this concentration of NCl_3 significantly exceeds the average ambient level (2.8 ppt) observed in a previous study (C. Wang et al., 2023). Such a high level of NCl_3 would also produce up to ~40 ppt of Cl_2 (Figure 7b), far exceeding the ambient levels of Cl_2 observed in our campaign. Moreover, assuming a similar detection limit of NCl_3 compared with other reactive chlorine species in this study, 16.3 ppt of NCl_3 should have been detectable by our Tof-CIMS. However, we could not unambiguously identify NCl_3 in our Tof-CIMS measurements. Alternatively, ~10 ppt of ICl could also compensate for the missing source of HOCl. However, the iodine atoms released by ICl photolysis would excessively deplete O_3 (Figure 7c). Considering the unrealistic outcomes of the photochemical degradation of NCl_3 and ICl, we conclude that other chlorine reservoirs are likely responsible for the missing sources of HOCl or Cl·. Nevertheless, we could not identify those potential chlorine reservoirs due to the limited understanding of chlorine chemistry.

Despite the unknown identity, we quantified the strength of the missing chlorine sources by hypothetically allocating those missing Cl· to the photolysis of additional Cl_2. Specifically, we increased the constrained Cl_2 levels to ~46 ppt (diurnal average) in the box model, achieving a balanced chemical budget of HOCl. Given that the ambient-observed Cl_2 mixing ratio is merely ~0.6 ppt (diurnal average), the missing chlorine sources are equivalent to 45.4 ppt Cl_2 in terms of their Cl· production rates. The implications of artificially augmenting 45.4 ppt of Cl_2 in the model are discussed in the subsequent section.

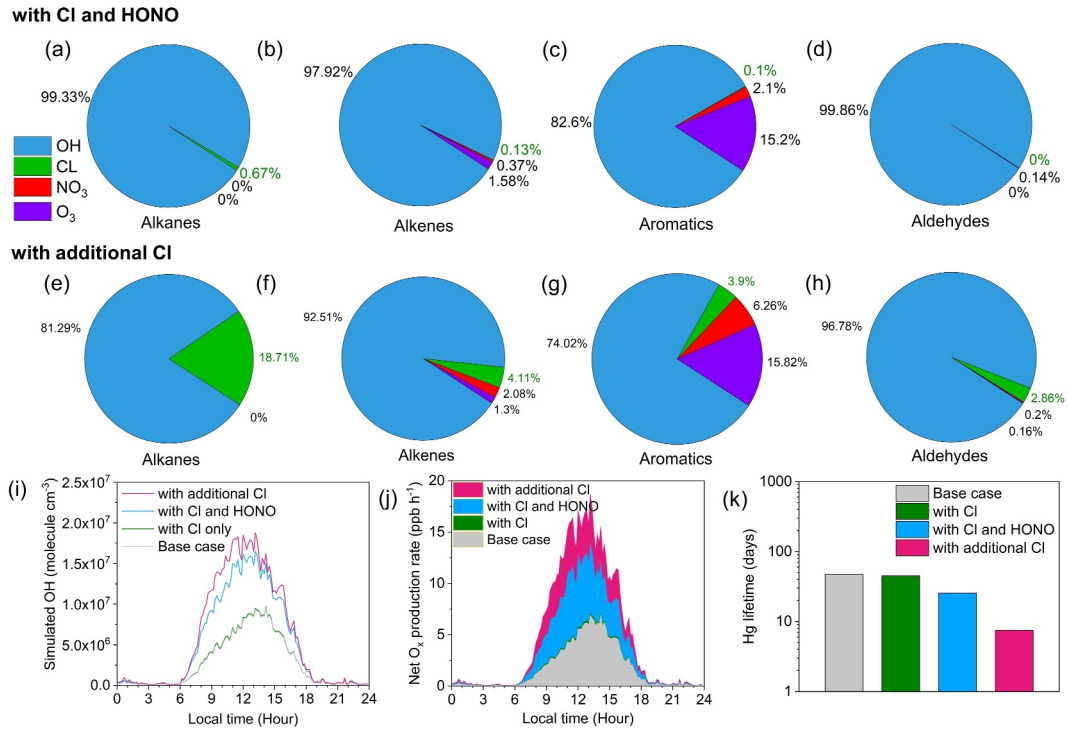

Figure 8. Impact of reactive chlorine on atmospheric oxidation capacity. (a)–(d) Contributions of different oxidants to the degradation of alkanes, alkenes, aromatics, and aldehydes, respectively, in the "with Cl and HONO" case. (e)–(h) The same as (a)–(d), but in the "with additional Cl" case. (i)–(k) Impact of reactive chlorine on the simulated OH· levels, net O_x production, and Hg^0 lifetime, respectively, in different simulation scenarios.

3.4. Implications for Atmospheric Oxidation Capacity

We evaluated the contribution of reactive chlorine to atmospheric oxidation capacity, comparing the relative importance of the observed chlorine reservoirs (i.e., $ClNO_2$, Cl_2, and HOCl) and HONO. Besides, we assessed the impact of potential chlorine sources required to balance the HOCl budget, which is equivalent to ~46 ppt of Cl_2 as mentioned previously. These impacts focus on VOC oxidation, OH· levels, the net O_x (O_3 + NO_2) production ($P(O_x)$), and the lifetime of Hg^0 and CH_4. Results show that OH· radicals dominate the oxidation of alkanes, alkenes, aromatics, and aldehydes (82.6%–99.9%, Figures 8a–8d), while Cl· radicals produced by known chlorine reservoirs contribute minimally to the oxidation of these VOCs, ranging from 0% to 0.67%. Although the rate constants of some Cl· + VOCs reactions are one to two orders of magnitude larger than those for OH· + VOCs reactions (Atkinson & Arey, 2003), the simulated level of OH· (~10^7 molecule cm^{-3} level) is four orders of magnitude larger than that of Cl· (~3×10^3 molecule cm^{-3} level) from the observed reactive chlorine. The high level of simulated OH· is partly attributable to HONO (~50% contribution), while Cl· chemistry barely increases OH· levels (Figure 8i). The additional OH· produced by HONO photolysis subsequently perturbs radical cycling, increasing RO_2· levels and contributing to $P(O_x)$ (Figure 8j). The high $P(O_x)$ implies a potential to produce high levels of O_3 in downwind coastal areas.

The enhanced atmospheric oxidation power owing to HONO also shortens the lifetime of Hg^0 and CH_4 (see the method part and Xia et al. (2022) for details). In the base case, excluding reactive chlorine or HONO, the Hg^0 lifetime is estimated to be 47.1 days (Figure 8k). The Hg^0 lifetime is slightly reduced to 45 days when incorporating reactive chlorine, while largely decreased to 25.6 days when both reactive chlorine and HONO are considered (Figure 8k). According to literature report, the Hg^0 lifetime ranged from 100 days to 1 year on a global scale while could be as short as 2 days (Peng et al., 2020) or even several hours (S. Wang et al., 2019; T. Wang et al., 2019) in specific regions with abundant reactive halogens. When the marine air masses associated with strong oxidation power encounter anthropogenic Hg^0 emissions in coastal areas, Hg^0 is converted into more reactive and toxic forms of mercury (Hg^{2+}), threatening aquatic ecosystems and human health through biomagnification (Zhang et al., 2021). Additionally, Cl· reduced the lifetime of CH_4 from 366 to 364 days, the impact

of which was negligible. It should be noted that the relative importance of Cl· can vary within a day, as the ratio of Cl· to OH· decreased from sunrise to sunset (Figure S9 in Supporting Information S1).

The significance of chlorine chemistry remarkably increases when the missing chlorine sources are considered. In the "with additional Cl" case, where ~46 ppt of Cl_2 is constrained to account for unknown reactive chlorine, the simulated Cl· level reaches up to 1.5 × 10^5 molecule cm^{-3} at noon. This Cl· concentration contributes significantly to the oxidation of VOCs (Figures 8e–8h), especially alkanes, with 18.7% contributions (Figure 7f). Additional Cl· from these unknown sources also raises the simulated OH· level to ~1.8 × 10^7 molecule cm^{-3} (Figure 8i) and $P(O_x)$ to up to 18 ppb h^{-1} (Figure 8j). The additional Cl· source also changes the response of the model-simulated OH· and $P(O_x)$ to environmental factors, especially NO_x, according to the sensitivity tests (Figure S10 in Supporting Information S1). The Hg^0 lifetime further decreases to below 10 days when the potential additional sources of chlorine are considered (Figure 8k). Additionally, the CH_4 lifetime further reduced from 364 to 321 days with additional chlorine, demonstrating a potential impact on climate. The impacts of chlorine chemistry with these additional chlorine sources are comparable to those observed at an urban site in North China (Ma et al., 2023) and a coastal site in south China (Niu et al., 2022), while they are less notable than those found in continental outflows in Hong Kong due to the higher levels of daytime Cl_2 (up to ~1 ppb) (Peng et al., 2022). This suggests that potential chlorine sources are significant, and further exploration of chlorine chemistry in the marine boundary layer is warranted.

4. Summary and Conclusion

Field observations coupled with box modeling are performed to probe the chlorine chemistry at a coastal site in Hong Kong under the influence of ship emissions. We observe clear daytime peaks of Cl_2 reaching several ppt level, which is probably formed by significant OH· uptake on aerosol and NO_3^- photolysis. Budget analysis of HOCl suggests the presence of missing chlorine sources in the ship emission plumes, which is equivalent to the Cl· produced by the photolysis of ~46 ppt Cl_2 (diurnal average). Newly reported chlorine species, that is, NCl_3 or ICl, could not explain the potential chlorine sources, pointing to unknown Cl· sources that remain to be resolved. The observed levels of reactive chlorine play a minor role in photochemistry, while the potentially additional Cl· sources could significantly promote atmospheric oxidation capacity. Overall, our findings highlight the need for further exploration of new chlorine sources under the influence of marine ship emissions.

Conflict of Interest

The authors declare no conflicts of interest relevant to this study.

Data Availability Statement

[Dataset] The Mendeley Data repository is used to access reactive chlorine species and related data measured in a field campaign in Hong Kong (https://data.mendeley.com/datasets/t77vw2s3tn/1). Research data used in this work are available in Xia (2024).

[Software] The box model used in this study is available online at https://github.com/AirChem/F0AM. The model code specific to this study, that is, the code to address iodine chemistry, is deposited permanently in the Mendeley Data repository in Xia (2025) (https://data.mendeley.com/datasets/5rzjzx9mfn/1). Figures in this work is created by Origin, which can be accessed under its license at https://www.originlab.com/.

Acknowledgments
We are grateful to the Hong Kong Environmental Protection Department for providing field measurement data of trace gases, aerosol mass concentrations, ionic compositions, VOCs, and OVOCs. We appreciate the Hong Kong Observatory to share the meteorological data. We acknowledge Douglas Worsnop, Xiaorui Chen, Zhouxing Zou, and Enyu Xiong for their helpful discussions. We thank Steven Poon for supporting the logistics and maintenance of the field station. This research was supported by the National Key Research and Development Program of China (2022YFC3701100) and the Hong Kong Research Grants Council (15217922 and T24-504/17-N). MX acknowledges support from the Wihuri Foundation.

References

Abbatt, J., Oldridge, N., Symington, A., Chukalovskiy, V., McWhinney, R. D., Sjostedt, S., & Cox, R. A. (2010). Release of gas-phase halogens by photolytic generation of OH in frozen Halide−Nitrate solutions: An active halogen formation mechanism? *The Journal of Physical Chemistry A*, *114*(23), 6527–6533. https://doi.org/10.1021/jp102072t

Ammann, M., Cox, R. A., Crowley, J. N., Jenkin, M. E., Mellouki, A., Rossi, M. J., et al. (2013). Evaluated kinetic and photochemical data for atmospheric chemistry: Volume VI—Heterogeneous reactions with liquid substrates. *Atmospheric Chemistry and Physics*, *13*(16), 8045–8228. https://doi.org/10.5194/acp-13-8045-2013

Atkinson, R., & Arey, J. (2003). Atmospheric degradation of volatile organic compounds. *Chemical Reviews*, *103*(12), 4605–4638. https://doi.org/10.1021/cr0206420

Atkinson, R., Baulch, D., Cox, R., Hampson Jr, R. F., Kerr, J., & Troe, J. (1989). Evaluated kinetic and photochemical data for atmospheric chemistry: Supplement III. IUPAC subcommittee on gas kinetic data evaluation for atmospheric chemistry. *Journal of Physical and Chemical Reference Data*, *18*(2), 881–1097. https://doi.org/10.1063/1.555832

Brown, S. S., Ryerson, T., Wollny, A., Brock, C., Peltier, R., Sullivan, A., et al. (2006). Variability in nocturnal nitrogen oxide processing and its role in regional air quality. *Science*, *311*(5757), 67–70. https://doi.org/10.1126/science.1120120

Brown, S. S., Stark, H., & Ravishankara, A. (2003). Applicability of the steady state approximation to the interpretation of atmospheric observations of NO_3 and N_2O_5. *Journal of Geophysical Research*, *108*(D17), 4539. https://doi.org/10.1029/2003jd003407

Burkholder, J. B. (1993). Ultraviolet absorption spectrum of HOCl. *Journal of Geophysical Research*, *98*(D2), 2963–2974. https://doi.org/10.1029/92jd02522

Chen, Q., Wang, X., Fu, X., Li, X., Alexander, B., Peng, X., et al. (2024). Impact of molecular chlorine production from aerosol iron photochemistry on atmospheric oxidative capacity in North China. *Environmental Science & Technology*, *58*(28), 12585–12597. https://doi.org/10.1021/acs.est.4c02534

Corbett, J. J., & Fischbeck, P. (1997). Emissions from ships. *Science*, *278*(5339), 823–824. https://doi.org/10.1126/science.278.5339.823

Dai, J., & Wang, T. (2021). Impact of international shipping emissions on ozone and $PM_{2.5}$ in East Asia during summer: The important role of HONO and $ClNO_2$. *Atmospheric Chemistry and Physics*, *21*(11), 8747–8759. https://doi.org/10.5194/acp-21-8747-2021

Eger, P. G., Friedrich, N., Schuladen, J., Shenolikar, J., Fischer, H., Tadic, I., et al. (2019). Shipborne measurements of $ClNO_2$ in the Mediterranean Sea and around the Arabian Peninsula during summer. *Atmospheric Chemistry and Physics*, *19*, 12121–12140. https://doi.org/10.5194/acp-19-12121-2019

Finlayson-Pitts, B., Ezell, M., & Pitts, J. (1989). Formation of chemically active chlorine compounds by reactions of atmospheric NaCl particles with gaseous N_2O_5 and $ClONO_2$. *Nature*, *337*(6204), 241–244. https://doi.org/10.1038/337241a0

Fountoukis, C., & Nenes, A. (2007). ISORROPIA II: A computationally efficient thermodynamic equilibrium model for K^+–Ca^{2+}–Mg^{2+}–NH_4^+–Na^+–SO_4^{2-}–NO_3^-–Cl^-–H_2O aerosols. *Atmospheric Chemistry and Physics*, *7*(17), 4639–4659. https://doi.org/10.5194/acp-7-4639-2007

Fu, H., Shang, G., Lin, J., Hu, Y., Hu, Q., Guo, L., et al. (2014). Fractional iron solubility of aerosol particles enhanced by biomass burning and ship emission in Shanghai, East China. *Science of the Total Environment*, *481*, 377–391. https://doi.org/10.1016/j.scitotenv.2014.01.118

Gu, R., Wang, W., Peng, X., Xia, M., Zhao, M., Zhang, Y., et al. (2022). Nitrous acid in the polluted coastal atmosphere of the South China Sea: Ship emissions, budgets, and impacts. *Science of the Total Environment*, *826*, 153692. https://doi.org/10.1016/j.scitotenv.2022.153692

Haskins, J. D., Lee, B. H., Lopez-Hilifiker, F. D., Peng, Q., Jaeglé, L., Reeves, J. M., et al. (2019). Observational constraints on the formation of Cl_2 from the reactive uptake of $ClNO_2$ on aerosols in the polluted marine boundary layer. *Journal of Geophysical Research: Atmospheres*, *124*(15), 8851–8869. https://doi.org/10.1029/2019jd030627

Heland, J., Kleffmann, J., Kurtenbach, R., & Wiesen, P. (2001). A new instrument to measure gaseous nitrous acid (HONO) in the atmosphere. *Environmental Science & Technology*, *35*(15), 3207–3212. https://doi.org/10.1021/es000303t

Jenkin, M., Young, J., & Rickard, A. (2015). The MCM v3. 3.1 degradation scheme for isoprene. *Atmospheric Chemistry and Physics*, *15*(20), 11433–11459. https://doi.org/10.5194/acp-15-11433-2015

Kim, M. J., Farmer, D. K., & Bertram, T. H. (2014). A controlling role for the air−sea interface in the chemical processing of reactive nitrogen in the coastal marine boundary layer. *Proceedings of the National Academy of Sciences of the United States of America*, *111*(11), 3943–3948. https://doi.org/10.1073/pnas.1318694111

Lawler, M. J., Sander, R., Carpenter, L. J., Lee, J. D., von Glasow, R., Sommariva, R., & Saltzman, E. S. (2011). HOCl and Cl_2 observations in marine air. *Atmospheric Chemistry and Physics*, *11*(15), 7617–7628. https://doi.org/10.5194/acp-11-7617-2011

Lee, B. H., Lopez-Hilfiker, F. D., Mohr, C., Kurtén, T., Worsnop, D. R., & Thornton, J. A. (2014). An iodide-adduct high-resolution time-of-flight chemical-ionization mass spectrometer: Application to atmospheric inorganic and organic compounds. *Environmental Science & Technology*, *48*(11), 6309–6317. https://doi.org/10.1021/es500362a

Li, Q., Fernandez, R. P., Hossaini, R., Iglesias-Suarez, F., Cuevas, C. A., Apel, E. C., et al. (2022). Reactive halogens increase the global methane lifetime and radiative forcing in the 21st century. *Nature Communications*, *13*(1), 2768. https://doi.org/10.1038/s41467-022-30456-8

Li, Q., Fu, X., Peng, X., Wang, W., Badia, A., Fernandez, R. P., et al. (2021). Halogens enhance haze pollution in China. *Environmental Science & Technology*, *55*(20), 13625–13637. https://doi.org/10.1021/acs.est.1c01949

Lim, M., Chiang, K., & Amal, R. (2006). Photochemical synthesis of chlorine gas from iron(III) and chloride solution. *Journal of Photochemistry and Photobiology A: Chemistry*, *183*(1–2), 126–132. https://doi.org/10.1016/j.jphotochem.2006.03.005

Ma, W., Chen, X., Xia, M., Liu, Y., Wang, Y., Zhang, Y., et al. (2023). Reactive chlorine species advancing the atmospheric oxidation capacities of inland urban environments. *Environmental Science & Technology*, *57*(39), 14638–14647. https://doi.org/10.1021/acs.est.3c05169

McNamara, S. M., Raso, A. R., Wang, S., Thanekar, S., Boone, E. J., Kolesar, K. R., et al. (2019). Springtime nitrogen oxide-influenced chlorine chemistry in the coastal Arctic. *Environmental Science & Technology*, *53*(14), 8057–8067. https://doi.org/10.1021/acs.est.9b01797

Molina, M. J., Tso, T.-L., Molina, L. T., & Wang, F. C.-Y. (1987). Antarctic stratospheric chemistry of chlorine nitrate, hydrogen chloride, and ice: Release of active chlorine. *Science*, *238*(4831), 1253–1257. https://doi.org/10.1126/science.238.4831.1253

Niu, Y.-B., Zhu, B., He, L.-Y., Wang, Z., Lin, X.-Y., Tang, M.-X., & Huang, X.-F. (2022). Fast nocturnal heterogeneous chemistry in a coastal background atmosphere and its implications for daytime photochemistry. *Journal of Geophysical Research: Atmospheres*, *127*(13), e2022JD036716. https://doi.org/10.1029/2022JD036716

Osthoff, H. D., Roberts, J. M., Ravishankara, A. R., Williams, E. J., Lerner, B. M., Sommariva, R., et al. (2008). High levels of nitryl chloride in the polluted subtropical marine boundary layer. *Nature Geoscience*, *1*(5), 324–328. https://doi.org/10.1038/ngeo177

Peng, X., Wang, T., Wang, W., Ravishankara, A. R., George, C., Xia, M., et al. (2022). Photodissociation of particulate nitrate as a source of daytime tropospheric Cl_2. *Nature Communications*, *13*(1), 939. https://doi.org/10.1038/s41467-022-28383-9

Peng, X., Wang, W., Xia, M., Chen, H., Ravishankara, A. R., Li, Q., et al. (2020). An unexpected large continental source of reactive bromine and chlorine with significant impact on wintertime air quality. *National Science Review*, *8*(7). https://doi.org/10.1093/nsr/nwaa304

Pratte, P., & Rossi, M. J. (2006). The heterogeneous kinetics of HOBr and HOCl on acidified sea salt and model aerosol at 40–90% relative humidity and ambient temperature. *Physical Chemistry Chemical Physics*, *8*(34), 3988–4001. https://doi.org/10.1039/b604321f

Riedel, T. P., Bertram, T. H., Crisp, T. A., Williams, E. J., Lerner, B. M., Vlasenko, A., et al. (2012). Nitryl chloride and molecular chlorine in the coastal marine boundary layer. *Environmental Science & Technology*, *46*(19), 10463–10470. https://doi.org/10.1021/es204632r

Roberts, J. M., Osthoff, H. D., Brown, S. S., & Ravishankara, A. (2008). N_2O_5 oxidizes chloride to Cl_2 in acidic atmospheric aerosol. *Science*, *321*(5892), 1059. https://doi.org/10.1126/science.1158777

Saiz-Lopez, A., Fernandez, R. P., Ordóñez, C., Kinnison, D. E., Gómez Martín, J. C., Lamarque, J. F., & Tilmes, S. (2014). Iodine chemistry in the troposphere and its effect on ozone. *Atmospheric Chemistry and Physics*, *14*(23), 13119–13143. https://doi.org/10.5194/acp-14-13119-2014

Simpson, W. R., Brown, S. S., Saiz-Lopez, A., Thornton, J. A., & von Glasow, R. (2015). Tropospheric halogen chemistry: Sources, cycling, and impacts. *Chemical Reviews*, *115*(10), 4035–4062. https://doi.org/10.1021/cr5006638

Solomon, S., Stone, K., Yu, P., Murphy, D. M., Kinnison, D., Ravishankara, A. R., & Wang, P. (2023). Chlorine activation and enhanced ozone depletion induced by wildfire aerosol. *Nature*, *615*(7951), 259–264. https://doi.org/10.1038/s41586-022-05683-0

Tham, Y. J., He, X.-C., Li, Q., Cuevas, C. A., Shen, J., Kalliokoski, J., et al. (2021). Direct field evidence of autocatalytic iodine release from atmospheric aerosol. *Proceedings of the National Academy of Sciences of the United States of America*, *118*(4), e2009951118. https://doi.org/10.1073/pnas.2009951118

Thornton, J. A., Kercher, J. P., Riedel, T. P., Wagner, N. L., Cozic, J., Holloway, J. S., et al. (2010). A large atomic chlorine source inferred from mid-continental reactive nitrogen chemistry. *Nature*, *464*(7286), 271–274. https://doi.org/10.1038/nature08905

Wang, C., Liggio, J., Wentzell, J. J. B., Jorga, S., Folkerson, A., & Abbatt, J. P. D. (2023). Chloramines as an important photochemical source of chlorine atoms in the urban atmosphere. *Proceedings of the National Academy of Sciences of the United States of America*, *120*(30), e2220889120. https://doi.org/10.1073/pnas.2220889120

Wang, L., Wen, L., Xu, C., Chen, J., Wang, X., Yang, L., et al. (2015). HONO and its potential source particulate nitrite at an urban site in North China during the cold season. *Science of the Total Environment*, *538*, 93–101. https://doi.org/10.1016/j.scitotenv.2015.08.032

Wang, S., McNamara, S. M., Moore, C. W., Obrist, D., Steffen, A., Shepson, P. B., et al. (2019). Direct detection of atmospheric atomic bromine leading to mercury and ozone depletion. *Proceedings of the National Academy of Sciences of the United States of America*, 201900613.

Wang, T., Dai, J., Lam, K. S., Nan Poon, C., & Brasseur, G. P. (2019). Twenty-five years of lower tropospheric ozone observations in tropical East Asia: The influence of emissions and weather patterns. *Geophysical Research Letters*, *46*(20), 11463–11470. https://doi.org/10.1029/2019gl084459

Wang, T., Tham, Y. J., Xue, L., Li, Q., Zha, Q., Wang, Z., et al. (2016). Observations of nitryl chloride and modeling its source and effect on ozone in the planetary boundary layer of southern China. *Journal of Geophysical Research: Atmospheres*, *121*(5), 2476–2489. https://doi.org/10.1002/2015jd024556

Wang, Y., Riva, M., Xie, H., Heikkinen, L., Schallhart, S., Zha, Q., et al. (2020). Formation of highly oxygenated organic molecules from chlorine-atom-initiated oxidation of alpha-pinene. *Atmospheric Chemistry and Physics*, *20*(8), 5145–5155. https://doi.org/10.5194/acp-20-5145-2020

Wang, Z., Wang, W., Tham, Y. J., Li, Q., Wang, H., Wen, L., et al. (2017). Fast heterogeneous N_2O_5 uptake and $ClNO_2$ production in power plant and industrial plumes observed in the nocturnal residual layer over the North China Plain. *Atmospheric Chemistry and Physics*, *17*(20), 12361–12378. https://doi.org/10.5194/acp-17-12361-2017

Wolfe, G. M., Marvin, M. R., Roberts, S. J., Travis, K. R., & Liao, J. (2016). The framework for 0-D atmospheric modeling (F0AM) v3. 1. *Geoscientific Model Development*, *9*, 3309–3319. https://doi.org/10.5194/gmd-9-3309-2016

Xia, M. (2024). Research data for the manuscript (2024JD042568) submitted to JGR: Atmospheres in 2024 [Dataset]. *Mendeley Data, V1*. https://doi.org/10.17632/t77vw2s3tn.1

Xia, M. (2025). Matlab code to address iodine chemistry discussed in the manuscript (2024JD042568) submitted to JGR: Atmospheres in 2024 [Software]. *Mendeley Data, V1*. https://doi.org/10.17632/5rzjzx9mfn.1

Xia, M., Peng, X., Wang, W., Yu, C., Sun, P., Li, Y., et al. (2020). Significant production of $ClNO_2$ and possible source of Cl_2 from N_2O_5 uptake at a suburban site in eastern China. *Atmospheric Chemistry and Physics*, *20*(10), 6147–6158. https://doi.org/10.5194/acp-20-6147-2020

Xia, M., Wang, T., Wang, Z., Chen, Y., Peng, X., Huo, Y., et al. (2022). Pollution-derived Br_2 boosts oxidation power of the coastal atmosphere. *Environmental Science & Technology*, *56*(17), 12055–12065. https://doi.org/10.1021/acs.est.2c02434

Yau, P., Lee, S., Corbett, J. J., Wang, C., Cheng, Y., & Ho, K. (2012). Estimation of exhaust emission from ocean-going vessels in Hong Kong. *Science of the Total Environment*, *431*, 299–306. https://doi.org/10.1016/j.scitotenv.2012.03.092

Ye, C., Gao, H., Zhang, N., & Zhou, X. (2016). Photolysis of nitric acid and nitrate on natural and artificial surfaces. *Environmental Science & Technology*, *50*(7), 3530–3536. https://doi.org/10.1021/acs.est.5b05032

Zhang, Y., Song, Z., Huang, S., Zhang, P., Peng, Y., Wu, P., et al. (2021). Global health effects of future atmospheric mercury emissions. *Nature Communications*, *12*(1), 3035. https://doi.org/10.1038/s41467-021-23391-7

Zhang, Y., Yang, X., Brown, R., Yang, L., Morawska, L., Ristovski, Z., et al. (2017). Shipping emissions and their impacts on air quality in China. *Science of the Total Environment*, *581–582*, 186–198. https://doi.org/10.1016/j.scitotenv.2016.12.098

Zheng, Z., Li, K., Xu, B., Dou, J., Li, L., Zhang, G., et al. (2023). O_3–precursor relationship over multiple patterns of timescale: A case study in Zibo, Shandong Province, China. *Atmospheric Chemistry and Physics*, *23*(4), 2649–2665. https://doi.org/10.5194/acp-23-2649-2023

References From the Supporting Information

Burkholder, J., Sander, S., Abbatt, J., Barker, J., Cappa, C., Crounse, J., et al. (2020). *Chemical kinetics and photochemical data for use in atmospheric studies; evaluation number 19*. Jet Propulsion Laboratory, National Aeronautics and Space Administration.

Clark, T., & Clyne, M. (1969). Kinetic mechanisms in nitrogen-chlorine radical systems. Part 1—The formation and detection of the NCl_2 and N_3 free radicals using time-resolved absorption spectrophotometry. *Transactions of the Faraday Society*, *65*(0), 2994–3004. https://doi.org/10.1039/tf9696502994

Lewis, E. R. (2008). An examination of Köhler theory resulting in an accurate expression for the equilibrium radius ratio of a hygroscopic aerosol particle valid up to and including relative humidity 100%. *Journal of Geophysical Research*, *113*, D03205. https://doi.org/10.1029/2007jd008590

Rubtsov, N. M. (1998). Kinetic mechanism and chemical oscillations in the branching chain decomposition of nitrogen trichloride. *Mendeleev Communications*, *8*(5), 173–176. https://doi.org/10.1070/mc1998v008n05abeh000948

Ye, C., Zhang, N., Gao, H., & Zhou, X. (2017). Photolysis of particulate nitrate as a source of HONO and NO_x. *Environmental Science & Technology*, *51*(12), 6849–6856. https://doi.org/10.1021/acs.est.7b00387